ORIGINAL PAPER

Cytoskeletal and motility changes in human umbilical cord MSCs associated with nuclear-cytoplasmic RhoA redistribution during replicative senescence

Danila Bobkov[1]* | Anastasia Polyanskaya[2]† | Anastasia Musorina[1]* | Ekaterina Lomert[1]* | Sergey Shabelnikov[1]* | Galina Poljanskaya[1]*

[1]Institute of Cytology of the Russian Academy of Science, 194064 Tikhoretsky ave. 4, St-Petersburg, Russia

[2]Peter the Great St. Petersburg Polytechnic University, Polytechnicheskaya, 29, St.Petersburg, 195251, Russia

Correspondence
Tikhoretsky ave. 4, St-Petersburg, 194064, Russia
Email: bobkov@incras.ru

Present address
† Peter the Great St. Petersburg Polytechnic University, Polytechnicheskaya, 29, St.Petersburg, 195251, Russia

Funding information
This research received no external funding.

One of the essential signs of replicative senescence is a decrease in cell motility. Here we provide evidence for changes in the organization of the contractile apparatus of human human umbilical cord MSCs in the process of replicative senescence. Using the automated system of intravital confocal cytometry and immunofluorescence based colocalization analisys the characteristics of cell motility and cytoskeleton organization were studied in MSCWJ-1 at various passages. The colocalization dynamics of myosin-9, α-actinin-4, and RhoA with F-actin and nuclei were examined. Result shows that RhoA nuclear-cytoplasmic redistribution correlates with cell motility changes, maximum RhoA nuclear localization was detected at passage 15. FPLC gel filtration of cytosolic extracts revealed myosin-9 assembly- incompetent form enrichment at passage 15. Quantitative analisys of MSCWJ-1 movements revealed decline in cell speed during cultivation accompanied by changes in tortuosity of

Abbreviations: DMEM, Dulbecco's modified Eagle's medium; FBS, fetus bovine serum; MSCs, mesenchymal stem cells; RCF, relative centrifugal force; PCA, principal component analisys; MSCWJ-1, human umbilical cord MSCs cell line; bTau, τ-Kendall rank correlation coefficient; Rs, Spearman's R correlation coefficient; tM, Manders correlation coefficient; Rval, Pearson correlation coefficient; FPLC, fast performance liquid chromatography

movements: tortuosity first increases at 15 passage and then decreases at 36 passage.

KEYWORDS
mesenchymal stem cells, *cellular senescense*, actin cytoskeleton, myosin-9, α-actinin-4, RhoA, cell motility

1 | INTRODUCTION

At present, the urgent task of cell biology is the isolation and comparative characterization of human MSCs isolated from various sources. The importance of such studies stems from the features of the interaction of MSCs isolated from different tissues, with their characteristic microenvironment. The origin or source of the MSC can determine their functional characteristics. Comparative analysis of the characteristics that are decisive in maintaining the status of MSCs, as well as a number of other characteristics responsible for the most important cellular processes, contributes to the deepening of basic knowledge of human MSCs, which is important both for understanding the mechanisms of biological processes in the cell and for expanding opportunities for using MSCs in regenerative medicine. Due to the importance of MSCs for the functioning of the body, the mechanisms of MSC interaction with damaged tissues and organs are widely studied. It has been shown that one of the most important mechanisms of action of various MSCs on damaged tissues is their ability to migrate to these sites and exert a trophic action due to the secretion of bioactive factors that alter the microenvironment of damaged cells and, thereby, improving tissue repair. At present, the mechanisms of tissue repair using MSCs related to the production of cytokines and paracrine factors are widely discussed in the literature (Phinney and Prockop (2007); Carvalho et al. (2011); Guiducci et al. (2011); Gruenloh et al. (2011); Huang et al. (2013); Luo et al. (2013); Ando et al. (2014); Hendijani et al. (2015b); Hendijani et al. (2015a); Danieli et al. (2016); Julianto and Rindastuti (2016); Teixeira et al. (2017); Vulcano et al. (2016); Zachar et al. (2016)).

Non-immortalized cell lines undergo a process of replicative senescence. Replicative senescence is a complex process that can begin at the early passages and gradually increase in the process of long-term cultivation. It is characterized by a significant decrease or cessation of proliferation, shortening of telomeres, morphological changes, increased β-galactosidase activity, increased expression of the tumor suppressor genes, decreased DNA repair and antioxidant activity of senescence cells, due to reduced expression of the corresponding genes, decreased differentiation potential, a number of epigenetic changes (Wagner et al. (2008); Kuilman et al. (2010); Redaelli et al. (2012); Estrada et al. (2013); Savickienė et al. (2016); Danisovic et al. (2017); Koltsova et al. (2018); Alessio et al. (2018); Krylova et al. (2018); Niedernhofer et al. (2018); Truong et al. (2018); Yu et al. (2018)). It is important to emphasize that senescence of MSCs may be associated not only with replicative senescence, which can be traced during prolonged passenescence of MSCs in vitro, but also with factors external to MSCs. Senescence mechanisms affect both MSCs and microenvironment. In this regard, it is the interaction of MSCs and the microenvironment that ensures the age characteristics of MSCs. One of the essential signs of replicative senescence is a decrease in cell motility or cell migration. Violation of migration processes contributes to the deterioration of tissue repair (Geißler et al. (2012); Bertolo et al. (2015); Turinetto et al. (2016); Zhang et al. (2018)). Therefore, to use MSCs in regenerative medicine, it is necessary to know the nature of the process of replicative senescence in a particular line.

In order to find out how much cellular senescence can interfere with use of cells in biomedical work, it is important to it is important to find out to what extent cell mobility is impaired during long-term cultivation. Cell migration occurs through close contact with the extracellular matrix, on which cells are spread, and depends on the organization

of the actin cytoskeleton. In this regard, it is essential to study the role of senescence in the organization of the cytoskeleton. Currently, studies on the effect of replicative senescence on cytoskeleton reorganization are at the stage of accumulation of experimental results. There are a number of works describing molecular mechanisms and functional changes during the reorganization of the cytoskeleton during replicative senescence in different human and animal cell types (Larsen et al. (2003); Le Clainche and Carlier (2008); Wang and Jang (2009); Geißler et al. (2012); Özcan et al. (2016); Turinetto et al. (2016); Moujaber et al. (2019)). It is of considerable interest to analyze the effect of replicative senescence on cell motility and the reorganization of the actin cytoskeleton in the human MSC line, which has not been used in detail in such studies. Actin cytoskeleton provide the driving forces for creating morphological diversity and the dynamics of mammalian cells (Vasiliev (1991)). Motor proteins, such as nonmuscle myosin isoforms, involved in maintaining cell shape, cell migration, interaction with the substrate and with other cells, processes of intracellular transport, as well as signalling and the regulation of gene expression (Omelchenko et al. (2002)).

In this work, we used MSCWJ-1 cells that were not previously investigated. Little is known about how the structural aspects of these cells are modified as a result of replicative senescence. Thus, the objective of this study is analysis of replicative senescence in the process of long-term cultivation of the MSCWJ-1 in connection whith the actin cytoskeleton state and the behavior of moving cells. To analyze the state of the actin cytoskeleton, we selected two structural and one regulatory actin-binding proteins, myosin-9 and α-actinin-4 as well as small GTPase RhoA.r Using immunofluorescence and confocal microscopy-based quantitative image cytometry techniques, we investigated changes in distribution of F-actin and actin-binding proteins in conjunction with the registration of parameters characterizing cell motility. In order to characterize the change in the composition of cytoplasmic protein complexes containing myosin-9 and beta-actin, we used liquid chromatography.

2 | RESULTS

2.1 | β-Galactosidase activity

In the process of WJMSC-1 cultivation, there was a change in the morphology of the cells, expressed in an increase in the size and degree of cell spreading. During long-term cultivation (passages 7–36) within each passage, the culture was filled by homogeneous cell populations of fibroblast-like cells. The results of β-galactosidase enzyme activity estimtion presented in the table 1. The proportion of stained cells naturally increases with passage number, which confirms the senescent status of WJMSC-1.

2.2 | Colocalization analysis

In order to follow the dynamics of the reorganization of the contractile apparatus during replicative senescence, we used the immunofluorescence method. Using polyclonal antibodies against myosin-9, we performed initial passage screening. Assuming that the cells in the neighboring passages are negligibly little different from each other, we fixed WJMSC-1 and analyzed the myosin-9/F-actin colocalization at passages: 7, 9, 12, 15, 18, 21, 25, 27, 28, 35, 36. The results presented in the figure 1. In all spread cells, staining for myosin-9 reveals a characteristic striated pattern. In addition to the striated pattern, myosin-9 was detected in lamellae as separate spots. An increased number of cells with such spots was detected in preparations fixed at passages 15–20. As can be seen in fig 3 (B) the colocalization of myosin-9 and F-actin decreases from high to moderate level during cultivation and reaches a minimum at passage 15. Then, the colocolization rises to a very high level at passage 28, after which it again decreases during passage of cultivation to passage 36, which was our last time point. The use of post hoc analysis revealed the most significant

differences between groups associated with a decrease in colocalization at 15 and 18 passages (fig 3, C). For further research, we decided that 9, 15, 28, and 36 passages would be key points.

The results of staining cells with α-actinin-4 in these passages are presented in Fig. 2. α-Actinin-4 as well as myosin-9 was detected in cells in the form of striated patterns, less pronounced than in myosin-9, but nevertheless quite distinguishable. We studied the colocalization α-actinin-4/F-actin and α-actinin-4/nuclei. The results are presented in Figure 2 (C), α-actinin-4/nuclei colocalization decreases from moderate level to weak when moving from 28 to 36 passages. The same decrease is observed in the transition from 9 to 15 passage in case of α-actinin-4/F-actin colocalization.

RhoA was detected in the nucleus, along the stress in the perinuclear region, diffusely in the cytoplasm at passage 9, mainly in the nucleus at passage 15. The colocalization of small GTPase RhoA with nuclei significantly increases from moderate to noticeable level while passage gone from 9 to 15, then decreases to the initial level at passage 28, and even more decreases to the weak level at passage 36 (Figure 3). It should be noted that in almost half of the cells, the coefficient takes negative values, which indicates the complete absence of colocalization.

For a more detailed study of the detected phenomenon of nuclear-cytoplasmic shuttle, we used the analysis of 3D models performed in the nuclear region. Figure 4 shows RhoA in the nucleus as 3D image slices based on Z-stacks. In the XZ sections, it is noticeable that at the 9th passage, RhoA is distributed partly in the nucleus and partly in the cytolasm, at the 15th passage for the most part inside the nucleus and in the perinuclear region, and at the 36th passage only along stress fibrils and in the cytoplasm.

2.3 | Trajectory analysis

The results of a quantitative analisys of 24-hour MSCWJ-1 movements show at figure 5. Fig.5 (A) show characteristic frames from time laps of cell movement recording over 24 hours. Cells are in sparse seeding, on each field of view several tracks are highlighted with colored lines. Statistical analisys of the obtained trajectories are presented in Fig.5 (B). Speed and path length significantly decreased with increase in passage number. At the same time, the total distance traveled significantly decreases only when switching from 9 to 15 passages and 15 passage does not differ from 36. The straightness of the trajectory increases significantly with the passage from passage 15 to 36. The tortuosity of the trajectory increases with the transition from passage 9 to 15 and then decreases by passage 36 to a level significantly lower than it was at passage 9. The numerical values obtained from the analysis are presented in the table 2.

2.4 | Gel chromatography

Chromatographic analysis results shown at Fig 6. Myosin-9 was detected at passage 9 mostly in high molecular weight fractions 3, 4, and to a lesser extent in fractions 7 and 9. At passage 15, the amount of myosin in fractions 3—-4 decreases, but the tail of the elution distribution is enriched: low molecular weight fractions are uniformly colored at a good signal level, starting from 10 to 14. At passage 36, myosin-9 is detected mainly in 3—4 fractions. β-Actin is detected mainly in the 10—11 fractions at passage 9. But at 15 and 36 passages it also revealed in fractions 6—7.

3 | DISCUSSION

Although a considerable amount of information is collected regarding replicative senescence senescence since Leonard Hayflick discovered that human cells cannot endlessly divide (Hayflick and Moorhead (1961)), little is known about the mechanisms of senescence in context of actin cytoskeleton rearrangements. Until now the cell motility characteristics has not been studied for senescent MSCs. All cells in culture are in constant motion. Small cells that have recently passed the stage of mitosis move very quickly. Apparently, the contribution of cells with a predominant amoeboid type of movement becomes so noticeable. Both external and intrinsic factors control directionality of cell movement Tiurin-Kuz'min et al. (2013). A number of actin-binding proteins prevent the depolymerization of F-actin microfilaments and regulate their stability, such as tropomyosins, α-actinins, for example.

Since myosin-9 is a key protein for cell migration, we investigated the distribution various passages. The actin cytoskeleton and its associated motor protein myosin-9 demonstrate characteristic striated pattern in in all studied passages, but at passages 15-17 among the variants of the spatial organization of the cytoskeleton, a spotty pattern becomes noticeable. Apparently, the accumulation of myosin-9 in light molecular weight fractions after gel filtration, which we observe at passage 15, is due to the fact that the protein is in the assembly-incompetent form (Vicente-Manzanares et al. (2009)), which is also consistent with immunofluorescence data, where we see the accumulation of actin-binding proteins in the form of individual particles, or multimolecular protein complexes. Mammalian nonmuscle myosin II is a kew protein in regulation cell motility Shutova and Svitkina (2018).

We assume that the detected changes in the localization of F-actin and actin-binding proteins reflect the phenomenon of partial disassembly of the cytoskeleton, which is characteristic for switching types of cell movement. It was shown that tropomyosins act as negative regulators of myosin stack formation Hu et al. (2019). In this regard, we decided to see how the interaction of α-actinin-4 with actin changes. We can interpret the spotted pattern observed at passage 15 in the case of myosin-9 and α-actinin-4, as a partial disassembly of the cytoskeletal structures. It is possible that switching from the mesenchymal type of movement and vice versa is mediated by the transfer of myosin-9 from one form to another and requires the presence of RhoA in the nucleus. α-Actinin-4 was found in nuclei in association with NF-κB transcription factor early in our laboratory (Babakov et al. (2008), Lomert et al. (2018), Bolshakova et al. (2007)). It was shown by An et al. (2016) α-Actinin-4 induces the epithelial-to-mesenchymal transition and tumorigenesis. In addition to regulating cell motility, this protein plays a role in carcinogenesis of different localization (Barbolina et al. (2008), Hsu and Kao (2013)).

Elliott et al. find that Rho/ROCK-stimulated myosin II contractility minimizes cell-scale branching by recognizing and minimizing local cell-surface curvature Elliott et al. (2015). Differences in the organization of the cytoskeleton in normal and cancer cells (Shutova and Alexandrova (2010)). The cell movement is based on the rearrangement of the actin cytoskeleton. The initial step of the rearrangements is the formation of the so-called leading (active) edge, at which protrusions take place and primary contacts of the cell with the extracellular matrix are formed. Smurf1 thus links the polarity complex to degradation of RhoA in lamellipodia and filopodia to prevent RhoA signaling during dynamic membrane movements Wang et al. (2003). Moving to the nucleus, RhoA can down-regulate stress fibrils organization and at the same time regulate a number of genes.

These data can be compared with the results of the analysis of cell motility, in which the sinuosity index reaches its maximum at passage 15, which indicates that such cells change direction of movement more often than young and old cells. Cytoskeleton isoactins form less stable polymers than skeletal muscle actin Khaitlina (2001).

4 | EXPERIMENTAL PROCEDURES

Trade names should be capitalized. The manufacturer's name should be followed by an address including town, (state, if USA) and country.

4.1 | Cell cultures: MSCWJ-1

A line of human mesenchymal stem cells obtained from Varton's jelly of the human umbilical cord (MSCWJ-1) were obtained from "Collection of vertebrate cell cultures" of the Institute of Cytology of the Russian Academy of Sciences (St. Petersburg, Russia). Main characteristics confirming the status of MSCs for MSCWJ-1, according to the requirements of the International Society for Cellular Therapy, were published previously (Dominici et al. (2006); Sensebe et al. (2010); Krylova et al. (2017)). MSCWJ-1 cells were cultured in growth medium containing 90% DMEM/F12 medium (Biolot, Russia) and 10% fetal bovine serum (FBS) (Hyclone, United States). Cells were cultured in 5% CO_2, $37^{\circ}C$ and 90% humidity conditions. Microbiological analysis confirmed the absence of bacterial, fungal and mycoplasmal contamination in the resulting line.

4.2 | Replicative cell senescence

The efficacy of the β-galactosidase enzyme was evaluated by the β-galactosidase enzyme activity. MSCWJ-1 cells were grown in 3.5 cm Petri dishes until subconfluent formation. Then the medium was removed and the cells were stained using a reagent kit (Senescence β-galactosidase staining kit; Cell Signaling, USA), according to the instructions. In cells entering the phase of replicative senescence, the cytoplasm has a bright blue color. The analysis was performed using an inverted microscope equipped with 60x objective (Nicon, Japan) on the 6th, 15th, 20th and 28th passages. The percentage of stained cells in percent was determined by counting at least 1000 cells in different fields of view at one time point. The results were processed statistically as described further.

4.3 | Immunofluorescence

Coverslips with adherent cells were fixed in a 3% solution of paraformaldehyde for 10 min at room temperature and permeabilized in a solution of 0.1% TritonX-100 for 10 min at room temperature, then the coverslips with cells was poured with 1% BSA solution for 20 min. Rabbit polyclonal antibodies produced against the N-terminal peptide of the heavy chain of nonmuscle myosin IIA, rabbit polyclonal antibodies produced against the α-actinin-4 and mouse monoclonal antibodies produced against the RhoA were used as the first antibodies. Goat antibodies to the Alexa fluor 488 rabbit antigens (Invitrogen, USA) were used as second antibodies. To visualize the actin cytoskeleton, cells were stained with rhodamine phalloidin for 20 min at room temperature and stained with DAPI with final concentration 1.5 μg/mL. Preparations were made on ProLong Gold antifade reagent containing. Cells were analyzed on a confocal microscope Leica SP8 (Germany).

4.4 | Colocalization analysis

Colocalization coefficients were calculated using ImageJ version 1.52i using the Coloc 2 plugin (Rueden et al. (2017)). Raw 1024 x 1024 px images was in 72 dpi resolution. For colocalization analysis images were opened in ImageJ, RGB channels were converted to 32 bit grayscale. Data collected in two channels from manually adjusted ROIs in confocal

images with MSCWJ-1 cells stained with polyclonal anti-myosin-9 antibodies and rhodamine phalloidin. Cells were fixed at passages: 7, 9, 12, 15, 18, 21, 25, 27, 28, 35, 36. Cells were selected manually on merged image and ROI passed to Coloc 2 plugin. The bTau, Rval, Rs, tM1, tM2 colocalization coefficients were calculated and passed as CSV files to R environment (Adler et al. (2008); Bergholm et al. (2010)).

We conducted PCA in order to identify the colocalization coefficient most suitable for our purposes. The results presented in Supplementary. Shortly, bTau and Rs coefficients shows very high correlation, tM1 and Rval coefficient shows moderate correlation. Kruskal-Wallis rank sum test results suggest that bTau reflects changes in colocalization so well. The PCA and factor analysis allowed us to conclude that bTau is the most suitable coefficient and in the future we use it for the analysis of cytoskeletal rearrangements.

In further analysis, the values of the bTau shown were interpreted in accordance with the Cheddock scale (see table 1 in Supplementary).

4.5 | Quantitative image cytometry and cell movement analysis

Comparative analysis of cell movement characteristics relative to replicative senescence was performed using time-lapse movies. For recording the movement of individual cells we used high-content Quantitative Image Cytometer CQ1 (Yokogawa, Japan) with spinning disk confocal technology (Sakashita et al. (2015)). Cells were plated on 6-well dishes and stained with Hoechst 33342 (Invitrogen, USA). Images were acquired during 24 h session with 405-nm laser and bright field illumination using 40x 0.95-NA dry objective lens. All images had a 2560 x 2160 pixel resolution, with a pixel size equivalent to 0.2 μm in x and y. A set of x-y coordinates were obtained from images in ImageJ software with Manual tracking plugin. Each cell was manually marked in the middle of the nucleus in each time point. Only cells satisfying the following conditions were noted: the cell must be in the field of view in all frames, the cell does not divide. Dividing cells were not counted. Trajectories were obtained from from a set of x-y coordinates. The resulting tracks were combined into a data frame and analyzed in the R environment using trajr package (McLean and Skowron Volponi (2018)), which is a sutable toolkit for the numerical characterisation and analysis of the trajectories of moving cells. Trajectory coordinates were read from a CSV data file, and then passed in to the trajectory analysis functions. Trajectorys was resampled to 15 min fixed step lenght by rediscretization function using the algorithm described by Bovet & Benhamou (Bovet and Benhamou (1988)). As a result of the analysis of the trajectories, we obtained the following parameters: total length of the trajectory, straight-line distance from the start to the end of the trajectory, mean and maximum speeds, straightness and sinuosity indexes. To measure the straightness, or conversely, tortuosity, of trajectories, we used two indexes. The simplest is straightness index and computed as D/L, where D is the distance from the start to the end of the trajectory, and L is the length of the trajectory. This straightness index is a number ranging from 0 to 1, where 1 indicates a straight line. The straightness index is considered to be a reliable measure of the efficiency of a directed walk, but inapplicable to random trajectories. The sinuosity index defined by Benhamou (Benhamou (2004)) may be an appropriate measure of the tortuosity of a random search path. Sinuosity is a function of the mean cosine of turning angles, and is a corrected form of the original sinuosity index defined by Bovet and Benhamou (Bovet and Benhamou (1988)).

4.6 | FPLC gel filtration

For gel-chromatographic separation of cell lysates, an FPLC system (Pharmacia) was used. Signal detection was performed using Millichrome A-02 detection unit. Elution was performed with elution buffer (150 mM NaCl, 50 mM Tris, pH 7.5, 0.02% NaN3). The column was calibrated with the set of proteins shown in Supplementary. We obtained cell

extracts by lysis from a monolayer cell culture grown on 14 Petri dishes 9 cm in diameter. In order to prevent the destruction of multimolecular protein complexes, in the first stage the medium in the plates was replaced with medium containing 10 μM formaldehyde, incubated for 10 minutes at 37° C, then a solution of glycine at a concentration of 1.875 g per 200 ml was added to each cup PBS, incubated for 5-7 min at 37° C. Subsequently, we washed the cups after glycine with a solution of PBS and poured 20 μl of protease inhibitor and 1 ml of lysis buffer was left for 1 min on ice. Next, the method of sequential selection of cell extract was collected in the ependorf 1 ml of the sample. The final stage of lizing was centrifugation for 10 min at 24000 RCF and freezing of the samples at -80 ° C. The protein extract was filtered and applied to the column in a volume of 500 μl. Fractions were collected on ice 1 ml each 2 min starting from time point determined by calibration set separation. For protein sedimentation, 100 μl of 0.15% DOX sodium deoxycholate was added to the collected fractions and mixed vigorously, incubated for 10 minutes in a refrigerator, then 100 μl of 50% TCA was added, mixed, incubated for 15 minutes in a freezer, and precipitated by centrifuging the protein for 30 minutes at 20000 G at +4° C. The supernatant was removed, and cold 100% acetone was added to the precipitate, mixed vigorously and incubated for 12 hours at −20° C. A repeated washing with acetone was done, and then the protein was precipitated by centrifugation for 15 min at 20000 G at +4° C, the supernatant was collected, the precipitate was dried, and 2-fold sample buffer was added to the precipitate (125 mM Tris-HCl, pH 6.8, 4% SDS, 10% glycerol, 0.006% bromo-phenol blue, 1.8% β-mercaptoethanol). Samples were heated for 10 minutes at 98° C, probes were stored at -20° C before electrophoretic separation.

4.7 | Electrophoresis and western blot

Proteins were separated by electrophoresis in a 12.5% polyacrylamide gel under denaturing conditions in the presence of SDS (Laemmli (1970)). After electrophoresis, the gel was stained with Coomassie brilliant blue or carried out by Western blotting (Towbin et al. (1979)). Protein transfer from the gel to the Immobilon-P membrane (Millipore, United States) was carried out in Tris-glycine buffer pH 8.3, containing 10% ethanol and 0.1% SDS. Western blotting was performed according to the ECL protocol (Amersham, USA). After transferring, the membrane was washed for 20 minutes with PBS containing 0.1% tween-20 and blocked non-specific binding sites with 5% non-fat dry milk diluted in PBS for 1 hour. The membrane was incubated with the first antibodies for 1 hour at room temperature three times. washed in PBS, stained with second antibodies for 1 h at room temperature. Rabbit polyclonal antibodies produced against the N-terminal peptide of myosin-9, mouse monoclonal antibodies produced against the beta-actin were used as the first antibodies. Rabbit antibodies to mouse antigens and goat antibodies to rabbit antigens conjugated with horseradish peroxidase (Sigma, USA) were used as second antibodies. To enhance the signal in western blotting, SuperSignal substrate (Thermo Scientific, USA) was used. Chemiluminescent radiation was recorded using a ChemiDoc system (Bio-Rad, USA).

4.8 | Description of statistical analysis methods

The study materials were subjected to statistical processing using the methods of parametric and non-parametric analysis. The accumulation, correction, systematization of the initial information were carried out in Microsoft Office Excel 2016 spreadsheets. Statistical analysis was done using the free software computing environment R v. 3.5.3 (Team et al. (2014)).

The data obtained from β-Galactosidase activity assay were computed following the Wilson method to obtain 95 % confidence intervals for binomial proportions (Wilson (1927)).

The data obtained from measurements of the colocalization coefficient were combined into variational series, in

which the arithmetic mean values (M) and standard deviations (SD) were calculated. PCA, generalized linear model and maximum-likelihood factor analysis were performed if R environment (Husson et al. (2010), Dobson and Barnett (2008), Lawley and Maxwell (1971)). In the course of all-pairs comparisons of colocalization data post hoc multiple testing corrections were used to adjust the P-values: Mann-Whitney rank test, Bonferroni method, Scheffe's, and Dunn's tests). The results were visualized using the free Python computing software environment and the scikit-posthocs package (Terpilowski (2019)).

The data obtained from trajectory analysis were cleaned: those observations that deviate from the 1st or 3rd quartile by more than one and a half interquartile range were considered outliers and deleted. Quantitative indicators were evaluated for compliance with the normal distribution, for this purpose, the Shapiro – Wilk criterion was used with $n > 170$ (Shapiro and Wilk (1965); Shapiro and Francia (1972)) as well as indicators of asymmetry and kurtosis. When comparing several samples of quantitative data with a distribution other than normal, Kruskal-Wallis criterion was used, which is a non-parametric alternative to single-factor analysis of variance (Kruskal and Wallis (1952)). In the event that the calculated value of the Kruskal-Wallis criterion exceeded the critical one, the differences in the indicators were considered statistically significant (Wilcoxon (1992)).

Data and scrips used to generate the analyses are available via data repository on Github : `https://github.com/Dan609/myo`.

Author contributions

Author1 and Author6 designed the research, analyzed the data, wrote the article. Author2 carried out immunofluorescence and western blotting. Author3 maintained cell line and made the β-galactosidase test. Author4 carried out introvital confocal microscopy. Author5 made the chromatographic separation.

Acknowledgements

We thank Drs. G. Schtein and M. Vorobyov for their help with confocal microscopy. We thank S. Boykov for assistance in computational trajectory analysis. We acknowledge I. Kropacheva, N. Bildjug, and A. Koltsova for their technical help and general support. We appreciate Dr. Edvard's help in language manuscript review.

Conflict of interest

The authors declare no conflict of interest.

References

Adler, J., Pagakis, S. and Parmryd, I. (2008) Replicate-based noise corrected correlation for accurate measurements of colocalization. *Journal of microscopy*, **230**, 121–133.

Alessio, N., Pipino, C., Mandatori, D., Di Tomo, P., Ferone, A., Marchiso, M., Melone, M. A., Peluso, G., Pandolfi, A. and Galderisi, U. (2018) Mesenchymal stromal cells from amniotic fluid are less prone to senescence compared to those obtained from bone marrow: an in vitro study. *Journal of cellular physiology*, **233**, 8996–9006.

An, H., Yoo, S. and Ko, J. (2016) α-actinin-4 induces the epithelial-to-mesenchymal transition and tumorigenesis via regulation of snail expression and β-catenin stabilization in cervical cancer. *Oncogene*, **35**, 5893.

Ando, Y., Matsubara, K., Ishikawa, J., Fujio, M., Shohara, R., Hibi, H., Ueda, M. and Yamamoto, A. (2014) Stem cell-conditioned medium accelerates distraction osteogenesis through multiple regenerative mechanisms. *Bone*, **61**, 82–90.

Babakov, V. N., Petukhova, O. A., Turoverova, L. V., Kropacheva, I. V., Tentler, D. G., Bolshakova, A. V., Podolskaya, E. P., Magnusson, K.-E. and Pinaev, G. P. (2008) Rela/nf-κb transcription factor associates with α-actinin-4. *Experimental cell research*, **314**, 1030–1038.

Barbolina, M. V., Adley, B. P., Kelly, D. L., Fought, A. J., Scholtens, D. M., Shea, L. D. and Stack, M. S. (2008) Motility-related actinin alpha-4 is associated with advanced and metastatic ovarian carcinoma. *Laboratory investigation*, **88**, 602.

Benhamou, S. (2004) How to reliably estimate the tortuosity of an animal's path:: straightness, sinuosity, or fractal dimension? *Journal of theoretical biology*, **229**, 209–220.

Bergholm, F., Adler, J. and Parmryd, I. (2010) Analysis of bias in the apparent correlation coefficient between image pairs corrupted by severe noise. *Journal of Mathematical Imaging and Vision*, **37**, 204–219.

Bertolo, A., Gemperli, A., Gruber, M., Gantenbein, B., Baur, M., Pötzel, T. and Stoyanov, J. (2015) In vitro cell motility as a potential mesenchymal stem cell marker for multipotency. *Stem cells translational medicine*, **4**, 84–90.

Bolshakova, A., Petukhova, O., Turoverova, L., Tentler, D., Babakov, V., Magnusson, K.-E. and Pinaev, G. (2007) Extracellular matrix proteins induce re-distribution of α-actinin-1 and α-actinin-4 in a431 cells. *Cell biology international*, **31**, 360–365.

Bovet, P. and Benhamou, S. (1988) Spatial analysis of animals' movements using a correlated random walk model. *Journal of theoretical biology*, **131**, 419–433.

Carvalho, M. M., Teixeira, G. F., Rui, R. L., Sousa, N. and J Salgado, A. (2011) Mesenchymal stem cells in the umbilical cord: phenotypic characterization, secretome and applications in central nervous system regenerative medicine. *Current stem cell research & therapy*, **6**, 221–228.

Danieli, P., Malpasso, G., Ciuffreda, M. C. and Gnecchi, M. (2016) Testing the paracrine properties of human mesenchymal stem cells using conditioned medium. In *Mesenchymal Stem Cells*, 445–456. Springer.

Danisovic, L., Oravcova, L., Krajciova, L., Varchulova Novakova, Z., Bohac, M., Varga, I. and Vojtassak, J. (2017) Effect of long-term culture on the biological and morphological characteristics of human adipose tissue-derived stem cells. *J Physiol Pharmacol*, **68**, 149–158.

Dobson, A. J. and Barnett, A. G. (2008) *An introduction to generalized linear models*. Chapman and Hall/CRC.

Dominici, M., Le Blanc, K., Mueller, I., Slaper-Cortenbach, I., Marini, F., Krause, D., Deans, R., Keating, A., Prockop, D. and Horwitz, E. (2006) Minimal criteria for defining multipotent mesenchymal stromal cells. the international society for cellular therapy position statement. *Cytotherapy*, **8**, 315–317.

Elliott, H., Fischer, R. S., Myers, K. A., Desai, R. A., Gao, L., Chen, C. S., Adelstein, R. S., Waterman, C. M. and Danuser, G. (2015) Myosin ii controls cellular branching morphogenesis and migration in three dimensions by minimizing cell-surface curvature. *Nature cell biology*, **17**, 137.

Estrada, J. C., Torres, Y., Benguria, A., Dopazo, A., Roche, E., Carrera-Quintanar, L., Pérez, R., Enriquez, J. A., Torres, R., Ramirez, J. C. et al. (2013) Human mesenchymal stem cell-replicative senescence and oxidative stress are closely linked to aneuploidy. *Cell death & disease*, **4**, e691.

Geißler, S., Textor, M., Kühnisch, J., Könnig, D., Klein, O., Ode, A., Pfitzner, T., Adjaye, J., Kasper, G. and Duda, G. N. (2012) Functional comparison of chronological and in vitro aging: differential role of the cytoskeleton and mitochondria in mesenchymal stromal cells. *PloS one*, **7**, e52700.

Gruenloh, W., Kambal, A., Sondergaard, C., McGee, J., Nacey, C., Kalomoiris, S., Pepper, K., Olson, S., Fierro, F. and Nolta, J. A. (2011) Characterization and in vivo testing of mesenchymal stem cells derived from human embryonic stem cells. *Tissue engineering Part A*, **17**, 1517–1525.

Guiducci, S., Manetti, M., Romano, E., Mazzanti, B., Ceccarelli, C., Dal Pozzo, S., Milia, A. F., Bellando-Randone, S., Fiori, G., Conforti, M. L. et al. (2011) Bone marrow-derived mesenchymal stem cells from early diffuse systemic sclerosis exhibit a paracrine machinery and stimulate angiogenesis in vitro. *Annals of the rheumatic diseases*, **70**.

Hayflick, L. and Moorhead, P. S. (1961) The serial cultivation of human diploid cell strains. *Experimental cell research*, **25**, 585–621.

Hendijani, F., Javanmard, S. H., Rafiee, L. and Sadeghi-Aliabadi, H. (2015a) Effect of human wharton's jelly mesenchymal stem cell secretome on proliferation, apoptosis and drug resistance of lung cancer cells. *Research in pharmaceutical sciences*, **10**, 134.

Hendijani, F., Javanmard, S. H. and Sadeghi-aliabadi, H. (2015b) Human wharton's jelly mesenchymal stem cell secretome display antiproliferative effect on leukemia cell line and produce additive cytotoxic effect in combination with doxorubicin. *Tissue and Cell*, **47**, 229–234.

Hsu, K.-S. and Kao, H.-Y. (2013) Alpha-actinin 4 and tumorigenesis of breast cancer. In *Vitamins & Hormones*, vol. 93, 323–351. Elsevier.

Hu, S., Grobe, H., Guo, Z., Wang, Y.-H., Doss, B. L., Pan, M., Ladoux, B., Bershadsky, A. D. and Zaidel-Bar, R. (2019) Reciprocal regulation of actomyosin organization and contractility in non-muscle cells by tropomyosins and alpha-actinins. *Molecular Biology of the Cell*, mbc–E19.

Huang, Y.-C., Leung, V. Y., Lu, W. W. and Luk, K. D. (2013) The effects of microenvironment in mesenchymal stem cell–based regeneration of intervertebral disc. *The Spine Journal*, **13**, 352–362.

Husson, F., Lê, S. and Pages, J. (2010) Exploratory multivariate analysis by example using r, volume 20105550 of chapman & hall/crc computer science & data analysis. *CRC Press*, **30**, 101–102.

Julianto, I. and Rindastuti, Y. (2016) Topical delivery of mesenchymal stem cells" secretomes" in wound repair. *Acta Medica Indonesiana*, **48**, 217–220.

Khaitlina, S. Y. (2001) Functional specificity of actin isoforms. *International Review of Cytology*, **202**, 35–98.

Koltsova, A., Krylova, T., Musorina, A., Zenin, V., Turilova, V., Yakovleva, T. and Poljanskaya, G. (2018) The dynamics of cell properties during long-term cultivation of two lines of mesenchymal stem cells derived from wharton's jelly of human umbilical cord. *Cell and Tissue Biology*, **12**, 7–19.

Kruskal, W. H. and Wallis, W. A. (1952) Use of ranks in one-criterion variance analysis. *Journal of the American statistical Association*, **47**, 583–621.

Krylova, T., Koltsova, A., Musorina, A., Zenin, V., Turilova, V., Yakovleva, T. and Poljanskaya, G. (2017) Derivation and characteristic of two lines of human mesenchymal stem cells, generated from the wharton's jelly of the human umbilical cord. *Tsitologiia*, **59**, 315–327.

Krylova, T., Musorina, A., Koltsova, A., Zenin, V., Turilova, V., Yakovleva, T. and Poljanskaya, G. (2018) Isolation and comparative characteristics of mesenchymal stem-cell lines derived from foreskin of two donors of similar age. *Cell and Tissue Biology*, **12**, 271–280.

Kuilman, T., Michaloglou, C., Mooi, W. J. and Peeper, D. S. (2010) The essence of senescence. *Genes & development*, **24**, 2463–2479.

Laemmli, U. K. (1970) Cleavage of structural proteins during the assembly of the head of bacteriophage t4. *nature*, **227**, 680.

Larsen, M., Tremblay, M. L. and Yamada, K. M. (2003) Phosphatases in cell–matrix adhesion and migration. *Nature reviews Molecular cell biology*, **4**, 700.

Lawley, D. N. and Maxwell, A. E. (1971) Factor analysis as statistical method. *Tech. rep.*

Le Clainche, C. and Carlier, M.-F. (2008) Regulation of actin assembly associated with protrusion and adhesion in cell migration. *Physiological reviews*, **88**, 489–513.

Lomert, E., Turoverova, L., Kriger, D., Aksenov, N. D., Nikotina, A. D., Petukhov, A., Mittenberg, A. G., Panyushev, N. V., Khotin, M., Volkov, K. et al. (2018) Co-expression of rela/p65 and actn4 induces apoptosis in non-small lung carcinoma cells. *Cell Cycle*, **17**, 616–626.

Luo, J., Zhao, X., Tan, Z., Su, Z., Meng, F. and Zhang, M. (2013) Mesenchymal-like progenitors derived from human embryonic stem cells promote recovery from acute kidney injury via paracrine actions. *Cytotherapy*, **15**, 649–662.

McLean, D. J. and Skowron Volponi, M. A. (2018) trajr: An r package for characterisation of animal trajectories. *Ethology*, **124**, 440–448.

Moujaber, O., Fishbein, F., Omran, N., Liang, Y., Colmegna, I., Presley, J. F. and Stochaj, U. (2019) Cellular senescence is associated with reorganization of the microtubule cytoskeleton. *Cellular and Molecular Life Sciences*, 1–15.

Niedernhofer, L. J., Gurkar, A. U., Wang, Y., Vijg, J., Hoeijmakers, J. H. and Robbins, P. D. (2018) Nuclear genomic instability and aging. *Annual review of biochemistry*, **87**, 295–322.

Omelchenko, T., Vasiliev, J., Gelfand, I., Feder, H. and Bonder, E. (2002) Mechanisms of polarization of the shape of fibroblasts and epitheliocytes: Separation of the roles of microtubules and rho-dependent actin–myosin contractility. *Proceedings of the National Academy of Sciences*, **99**, 10452–10457.

Özcan, S., Alessio, N., Acar, M. B., Mert, E., Omerli, F., Peluso, G. and Galderisi, U. (2016) Unbiased analysis of senescence associated secretory phenotype (sasp) to identify common components following different genotoxic stresses. *Aging (Albany NY)*, **8**, 1316.

Phinney, D. G. and Prockop, D. J. (2007) Concise review: mesenchymal stem/multipotent stromal cells: the state of transdifferentiation and modes of tissue repair—current views. *Stem cells*, **25**, 2896–2902.

Redaelli, S., Bentivegna, A., Foudah, D., Miloso, M., Redondo, J., Riva, G., Baronchelli, S., Dalprà, L. and Tredici, G. (2012) From cytogenomic to epigenomic profiles: monitoring the biologic behavior of in vitro cultured human bone marrow mesenchymal stem cells. *Stem cell research & therapy*, **3**, 47.

Rueden, C. T., Schindelin, J., Hiner, M. C., DeZonia, B. E., Walter, A. E., Arena, E. T. and Eliceiri, K. W. (2017) Imagej2: Imagej for the next generation of scientific image data. *BMC bioinformatics*, **18**, 529.

Sakashita, H., Ohashi, K., Ozawa, K. and Tsubouchi, Y. (2015) The cq1 confocal quantitative image cytometer and its application to biological measurement. *Tech. rep.*, Yokogawa Technical Report English Edition.

Savickienė, J., Baronaitė, S., Zentelytė, A., Treigytė, G. and Navakauskienė, R. (2016) Senescence-associated molecular and epigenetic alterations in mesenchymal stem cell cultures from amniotic fluid of normal and fetus-affected pregnancy. *Stem cells international*, **2016**.

Sensebe, L., Krampera, M., Schrezenmeier, H., Bourin, P. and Giordano, R. (2010) Mesenchymal stem cells for clinical application. *Vox sanguinis*, **98**, 93–107.

Shapiro, S. S. and Francia, R. (1972) An approximate analysis of variance test for normality. *Journal of the American Statistical Association*, **67**, 215–216.

Shapiro, S. S. and Wilk, M. B. (1965) An analysis of variance test for normality (complete samples). *Biometrika*, **52**, 591–611.

Shutova, M. and Alexandrova, A. Y. (2010) Normal and transformed fibroblast spreading: Role of microfilament polymerization and actin-myosin contractility. *Cell and Tissue Biology*, **4**, 25–35.

Shutova, M. S. and Svitkina, T. M. (2018) Mammalian nonmuscle myosin ii comes in three flavors. *Biochemical and biophysical research communications*, **506**, 394–402.

Team, R. C. et al. (2014) R: A language and environment for statistical computing. *R*.

Teixeira, F. G., Carvalho, M. M., Panchalingam, K. M., Rodrigues, A. J., Mendes-Pinheiro, B., Anjo, S., Manadas, B., Behie, L. A., Sousa, N. and Salgado, A. J. (2017) Impact of the secretome of human mesenchymal stem cells on brain structure and animal behavior in a rat model of parkinson's disease. *Stem cells translational medicine*, **6**, 634–646.

Terpilowski, M. (2019) scikit-posthocs: Pairwise multiple comparison tests in python. *The Journal of Open Source Software*, **4**, 1169.

Tiurin-Kuz'min, P., Vorotnikov, A. and Tkachuk, V. (2013) Molecular mechanisms of gradient sensing in mesenchymal cells. *Rossiiskii fiziologicheskii zhurnal imeni IM Sechenova*, **99**, 294–312.

Towbin, H., Staehelin, T. and Gordon, J. (1979) Electrophoretic transfer of proteins from polyacrylamide gels to nitrocellulose sheets: procedure and some applications. *Proceedings of the National Academy of Sciences*, **76**, 4350–4354.

Truong, N. C., Bui, K. H.-T. and Van Pham, P. (2018) Characterization of senescence of human adipose-derived stem cells after long-term expansion.

Turinetto, V., Vitale, E. and Giachino, C. (2016) Senescence in human mesenchymal stem cells: functional changes and implications in stem cell-based therapy. *International journal of molecular sciences*, **17**, 1164.

Vasiliev, J. (1991) Polarization of pseudopodial activities: cytoskeletal mechanisms. *Journal of Cell Science*, **98**, 1–4.

Vicente-Manzanares, M., Ma, X., Adelstein, R. S. and Horwitz, A. R. (2009) Non-muscle myosin ii takes centre stage in cell adhesion and migration. *Nature reviews Molecular cell biology*, **10**, 778.

Vulcano, F., Milazzo, L., Ciccarelli, C., Eramo, A., Sette, G., Mauro, A., Macioce, G., Martinelli, A., La Torre, R., Casalbore, P. et al. (2016) Wharton's jelly mesenchymal stromal cells have contrasting effects on proliferation and phenotype of cancer stem cells from different subtypes of lung cancer. *Experimental cell research*, **345**, 190–198.

Wagner, W., Horn, P., Castoldi, M., Diehlmann, A., Bork, S., Saffrich, R., Benes, V., Blake, J., Pfister, S., Eckstein, V. et al. (2008) Replicative senescence of mesenchymal stem cells: a continuous and organized process. *PloS one*, **3**, e2213.

Wang, D. and Jang, D.-J. (2009) Protein kinase ck2 regulates cytoskeletal reorganization during ionizing radiation–induced senescence of human mesenchymal stem cells. *Cancer research*, **69**, 8200–8207.

Wang, H.-R., Zhang, Y., Ozdamar, B., Ogunjimi, A. A., Alexandrova, E., Thomsen, G. H. and Wrana, J. L. (2003) Regulation of cell polarity and protrusion formation by targeting rhoa for degradation. *Science*, **302**, 1775–1779.

Wilcoxon, F. (1992) Individual comparisons by ranking methods. In *Breakthroughs in statistics*, 196–202. Springer.

Wilson, E. B. (1927) Probable inference, the law of succession, and statistical inference. *Journal of the American Statistical Association*, **22**, 209–212.

Yu, J., Shi, J., Zhang, Y., Zhang, Y., Huang, Y., Chen, Z. and Yang, J. (2018) The replicative senescent mesenchymal stem/stromal cells defect in dna damage response and anti-oxidative capacity. *International journal of medical sciences*, **15**, 771.

Zachar, L., Bačenková, D. and Rosocha, J. (2016) Activation, homing, and role of the mesenchymal stem cells in the inflammatory environment. *Journal of inflammation research*, **9**, 231.

Zhang, T., Wang, P., Liu, Y., Zhou, J., Shi, Z., Cheng, K., Huang, T., Wang, X., Yang, G. L., Yang, B. et al. (2018) Overexpression of foxq1 enhances anti-senescence and migration effects of human umbilical cord mesenchymal stem cells in vitro and in vivo. *Cell and tissue research*, **373**, 379–393.

Supporting Information

Supplementary statistical tests results. Video files with cell tracking.

TABLE 1 β-galactosidase enzyme activity in MSCWJ-1 cells with limits of the 95% confidence interval

Passage Number	Cells stained,%	Cell count
9	6.02 ± 0.72	3724
15	20.55 ± 1.57	2404
20	26.28 ± 2.46	1149
28	43.97 ± 2.72	1260

TABLE 2 24 h cell movement trajectory analysis. Mean ± SD

Passage	Mean Speed, μm/h	Max Speed, μm/h	Length, μm	Distance, μm
9	38.3 ± 15.2	164.9 ± 56.4	911.3 ± 362.4	278.2 ± 169.8
15	25.0 ± 11.1	127.9 ± 59.3	595.1 ± 263.4	211.7 ± 162.8
36	18.3 ± 7.7	57.1 ± 27.8	431.6 ± 174.5	215.1 ± 156.4

Tables

Figure legends

Figures

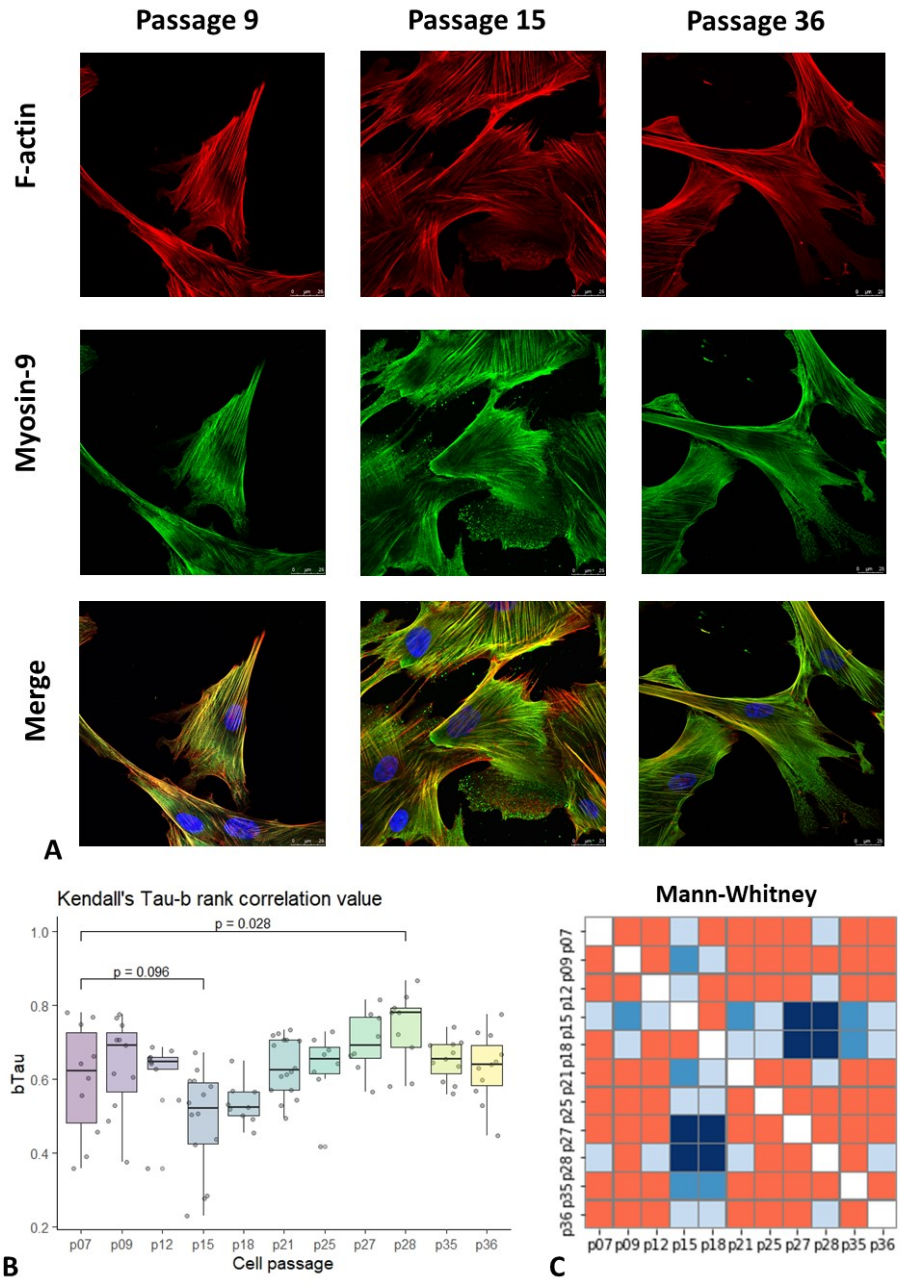

FIGURE 1 (A) Staining of F-actin (red) and myosin-9 (green) in WJMSC-1 at passages 9, 15, 36. (B) Myosin-9/F-actin colocalization in MSCWJ-1 at passages 7, 9, 12, 15, 18, 21, 25, 27, 28, 35, 36. Boxplots with means indicated by horizontal lines shown over jitter plots, each point indicate one observation. Significant differences identified by the Wilcoxon test are indicated by p-values. (C) Multiple Pairwise comparison test for the same data as shown in (B)

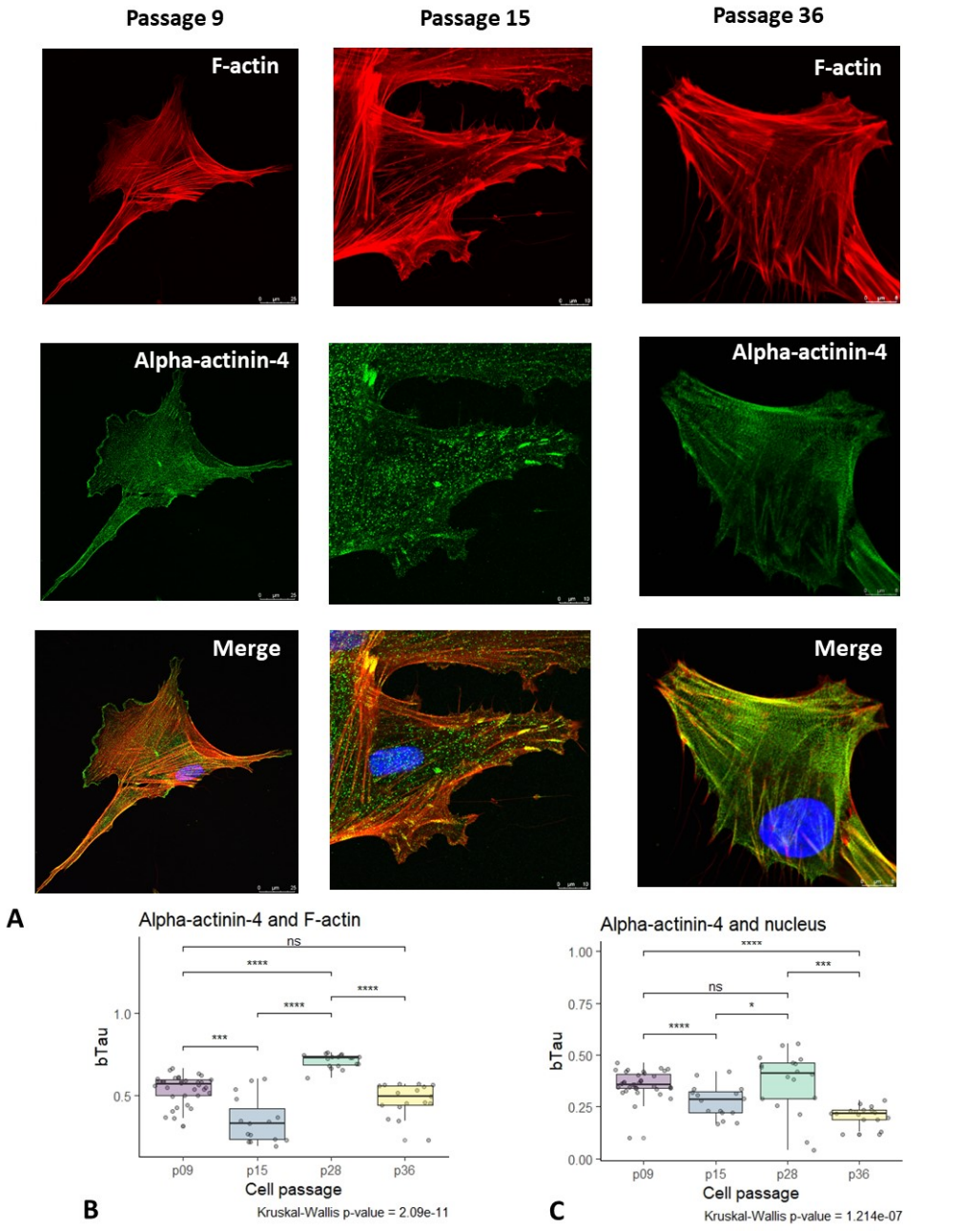

FIGURE 2 (A) Staining of F-actin (red) and α-actintin-4 (green). (B) α-actintin-4/F-actin colocolization at passages 9, 15, 28, 36. Boxplots with means indicated by horizontal lines shown over jitter plots, each point indicate one observation. Significant differences identified by the Wilcoxon test are indicated by asterisks. ns — not significant. Kruskal-Wallis test p-value is indicated. (C) α-actintin-4/nucleus colocolization at passages 9, 15, 28, 36. Boxplots with means indicated by horizontal lines shown over jitter plots, each point indicate one observation. Significant differences identified by the Wilcoxon test are indicated by asterisks. ns — not significant. Kruskal-Wallis test p-value is indicated.

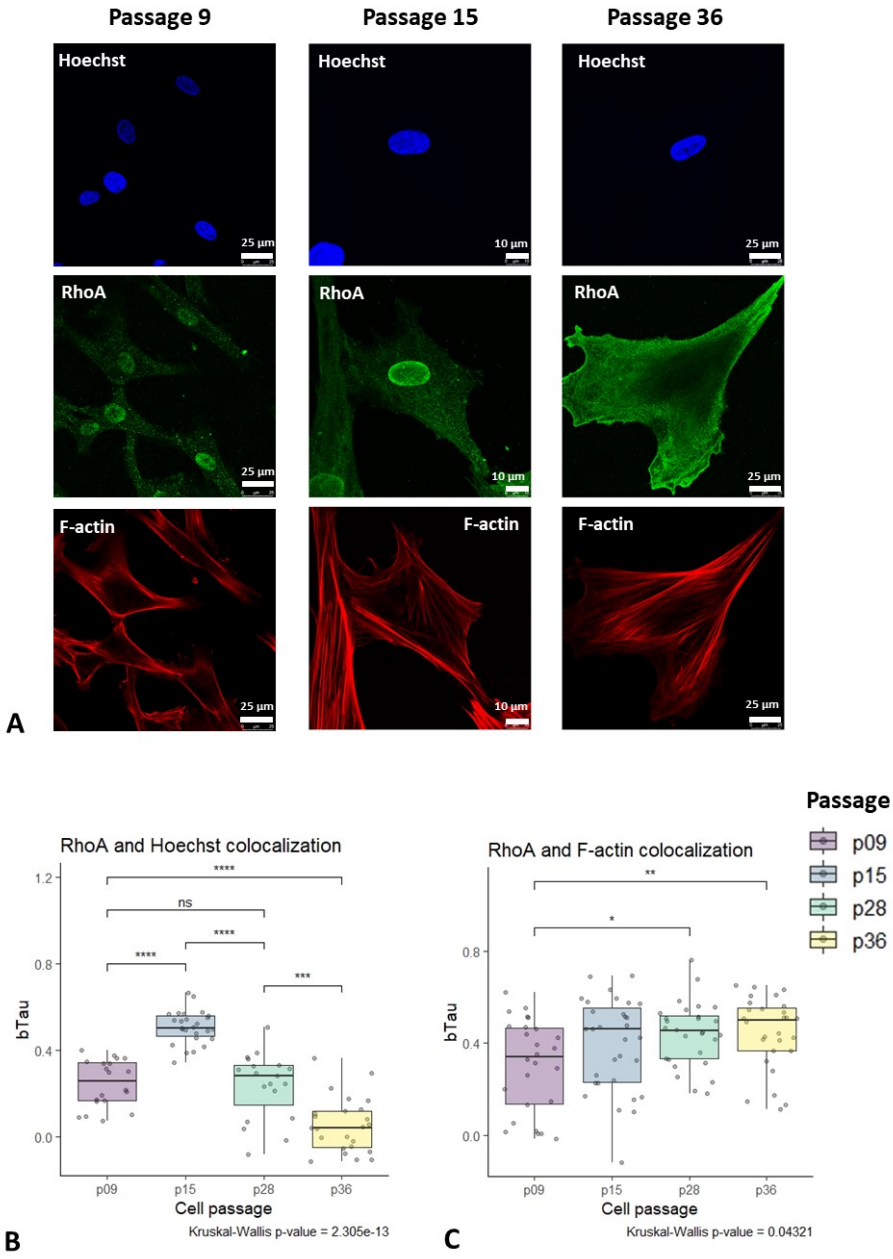

FIGURE 3 (A) Cell stained with polyclonal antibodies against RhoA (green), rhodamine-phalloidin (red), and Hoechst33342 (blue). WJMSC-1 fixed at passages 9, 15, and 36. (B) RhoA/nucleus colocalization. WJMSC-1 fixed at passages 9, 15, 28 and 36. Boxplots with means indicated by horizontal lines shown over jitter plots, each point indicate one observation. Significant differences identified by the Wilcoxon test are indicated by asterisks. ns — not significant. Kruskal-Wallis test p-value is indicated. (C) RhoA/F-actin colocalization. WJMSC-1 fixed at passages 9, 15, 28 and 36. Boxplots with means indicated by horizontal lines shown over jitter plots, each point indicate one observation. Significant differences identified by the Wilcoxon test are indicated by asterisks. Kruskal-Wallis test p-value is indicated.

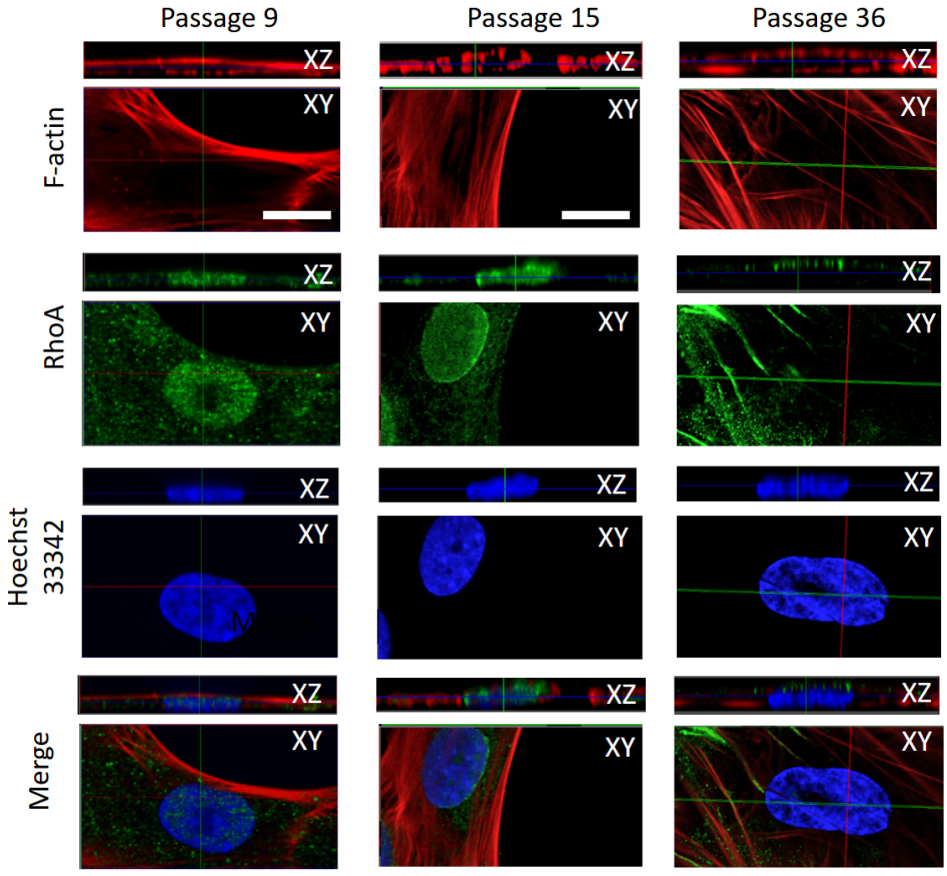

FIGURE 4 Confocal view of RhoA in the nucleus. WJMSC-1 fixed and permeabilized at passages 9, 15, and 36. Cell stained with polyclonal antibodies against RhoA (green), rhodamine-phalloidin (red), and Hoechst33342 (blue). 70 confocal optical sections were used to generate 3D image, slices show sections passing through the nucleus.

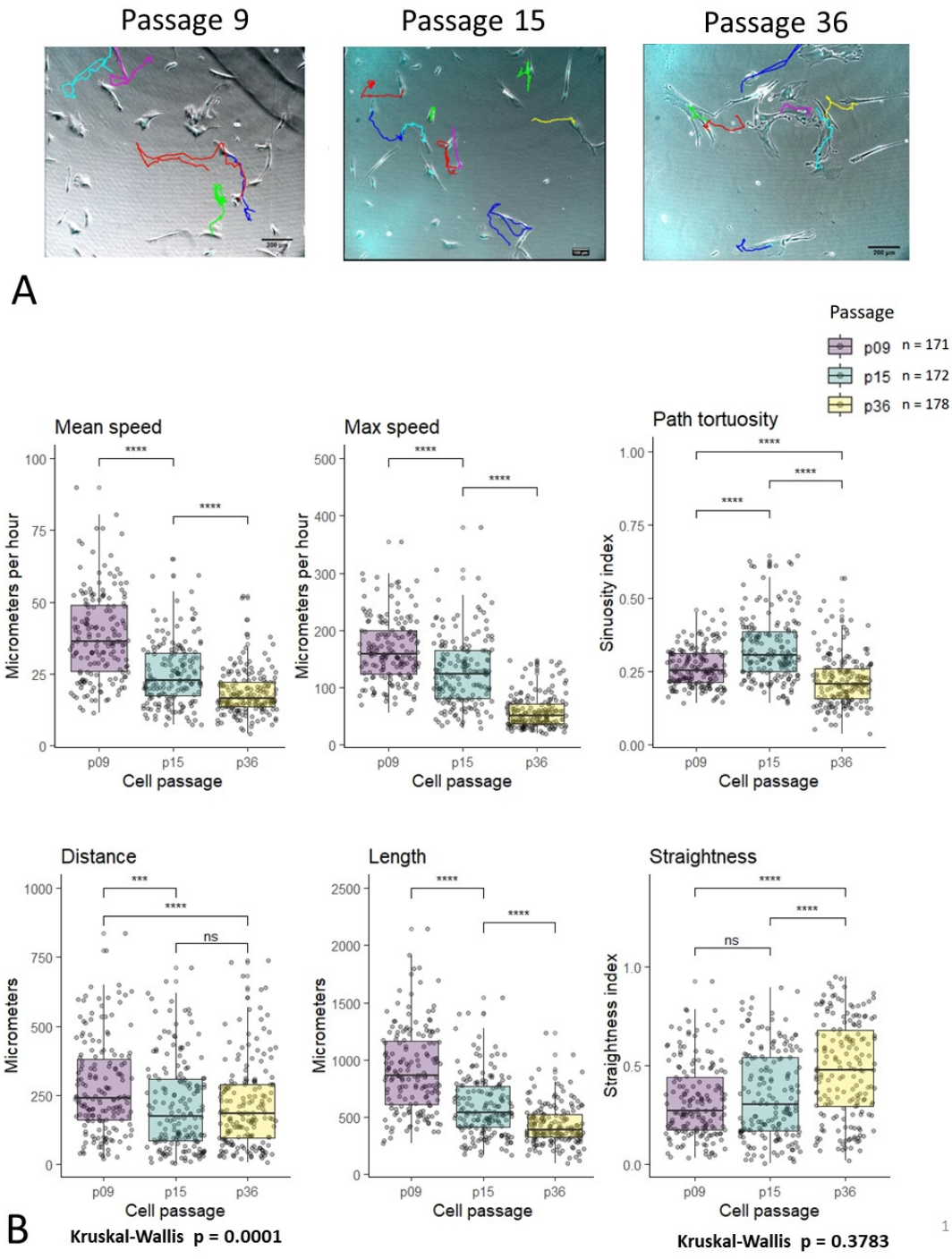

FIGURE 5 Cell movement analisys performed on 24 h confocal cytometry imaging. Cells were imaged at passages 9, 15, 36 (A) Characteristic images from trajectory analisys workflow. (B) Statistical analisys of calculated trajectories. Boxplots with Means indicated by horizontal lines shown over jitter plots, each point indicate one observation. Kruskal-Wallis test p-values are indicated only where $p > 0.00001$. Significant differences identified by the Wilcoxon test are indicated by asterisks. ns — not significant.

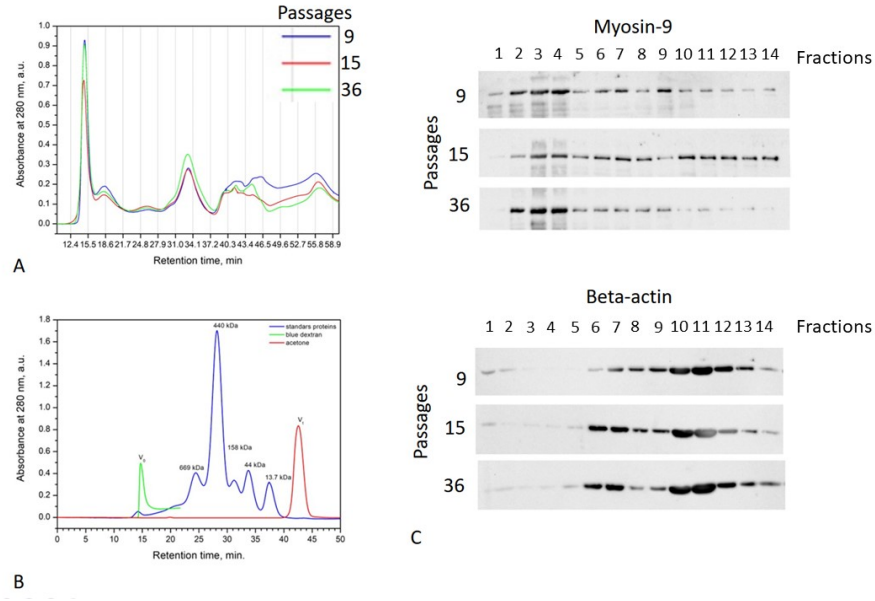

FIGURE 6 Gel chromatographic separation of cytoplasmic extracts from MSCWJ-1 at different stages of replicative senescence. Separation of calibration proteins (B) and comparison of elution profiles (A) are presented. (C) Electrophoretic separation and western blot detection of myosin-9 and β-actin in fractions obtained as a result of gel-chromatographic separation of cytoplasmic extracts from WJMSC1 cells at passages 9, 15, 36.